nitude. This is understood as follows: The quantum efficiency for radiative recombination of the exciton–neutral-sulfur complex is only about 1 : 500, because there is a much faster nonradiative Auger process.[15] Thus a decrease in the integrated intensity of the relatively sharp C line (which has no significant sidebands) could well account for the increase in the integrated intensity of the A line and its sidebands.

ACKNOWLEDGMENT

We would especially like to thank William Hawk for two of the samples.

*Work supported by National Science Foundation Grant No. GH 32401.

[1]P. J. Dean and D. G. Thomas, Phys. Rev. 150, 690 (1966).

[2]D. G. Thomas and J. J. Hopfield, Phys. Rev. 150, 680 (1966).

[3]D. G. Thomas, M. Gershenzon, and J. J. Hopfield, Phys. Rev. 131, 2397 (1963).

[4]F. A. Trumbore, M. Gershenzon, and D. G. Thomas, Appl. Phys. Letters 9, 4 (1966).

[5]See, for example, P. J. Dean, Phys. Rev. 157, 655 (1967); P. J. Dean, R. A. Faulkner, S. Kimura, and M. Ilegems, Phys. Rev. B 4, 1926 (1971).

[6]The hole has an angular momentum of $j=\frac{3}{2}$ and the electron $j=\frac{1}{2}$. The A line is from the $j=1$ level and the B line is from the $j=2$ level, at 5355 and 5357 Å, respectively. See Y. Yafet and D. G. Thomas, Phys. Rev. 131, 2405 (1963).

[7]Quenching of the sulfur C line by red light is reported in Ref. 3. Photodissociation of deep donor levels is reported by V. S. Aleksandrova, I. S. Gorban, and V. P. Zakharov, Fiz. Tverd. Tela 12, 2139 (1970) [Sov. Phys. Solid State 12, 1700 (1971)].

[8]M. J. Colles and J. A. Giordmaine, Phys. Rev. Letters 27, 670 (1971). These authors report evidence of phonon breakdown through a change in the intensity of fluorescence of a phonon sideband of a bound exciton in diamond. The effect is reported only for the anti-Stokes sideband, and a decrease rather than an increase of intensity is reported.

[9]The experiment and further elaboration on the experimental apparatus are described by M. Gundersen, Ph.D. thesis (University of Southern California, 1972) (unpublished).

[10]J. D. Cuthbert and D. G. Thomas, Phys. Rev. 154, 763 (1967).

[11]D. A. Kleinman and W. G. Spitzer, Phys. Rev. 118, 110 (1960).

[12]W. G. Harter (private communication).

[13]W. L. Faust and C. H. Henry, Phys. Rev. Letters 17, 1265 (1966).

[14]M. Gundersen and W. L. Faust, J. Appl. Phys. 44, 376 (1973).

[15]D. F. Nelson, J. D. Cuthbert, P. J. Dean, and D. G. Thomas, Phys. Rev. Letters 17, 1262 (1966).

PHYSICAL REVIEW B VOLUME 7, NUMBER 8 15 APRIL 1973

Multiphonon Raman Spectrum of Silicon*

Paul A. Temple† and C. E. Hathaway
Department of Physics, Kansas State University, Manhattan, Kansas 66502
(Received 20 December 1971)

The energy and polarization characteristics of the one- and two-phonon Raman spectrum have been measured using a 180° backscattering technique. The two-phonon spectrum was measured at 20, 80, and 305 °K. The one-phonon spectrum was measured at 17, 30, 80, and 305 °K. The one-phonon line of symmetry $\Gamma_{25'}$ was shown to be Lorentzian and to have a deconvoluted half-width at 17 °K of 1.45 ± 0.05 cm^{-1}. The two-phonon Raman spectrum was used to determine phonon energies at the four critical points Γ, X, L, and W.

INTRODUCTION

The lattice dynamics of materials having the diamond structure have been the subject of much experimental investigation. The phonon spectra of diamond, silicon, and germanium have all been investigated by inelastic neutron scattering[1–4] and by infrared absorption.[5–7] In addition, the phonon spectrum of diamond has been investigated by two-phonon Raman scattering.[8] The infrared-absorption spectrum of silicon was studied by Johnson[5] before neutron scattering data for silicon were available and by Johnson and Loudon[6] and by Balkanski and Nusimovici[7] after neutron data of Dolling[1] and Dolling and Cowley[9] were available. The dispersion curves obtained from these neutron data are shown in Fig. 1. The various phonon energies at the critical points Γ, X, L, and W, as indicated on the Brillouin zone shown in Fig. 2, were assigned by Balkanski and Nusimovici using the infrared-absorption data and the inelastic neutron scattering data. Both of these efforts made use of

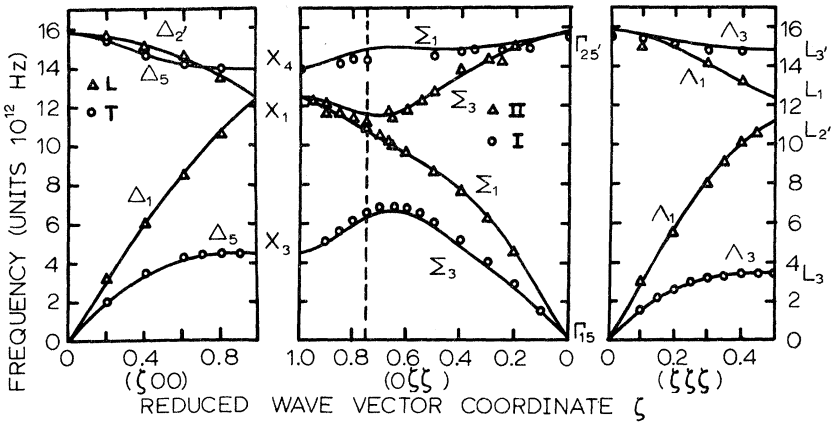

FIG. 1. The dispersion curves for silicon obtained by Dolling (Refs. 1 and 33).

the work of Van Hove[10] and of Phillips[11,12] for determining the expected shapes of features in the infrared-absorption spectrum.

Silicon possesses the diamond structure O_h^7 ($Fd3m$) and therefore has only one first-order Raman-active phonon of symmetry $\Gamma_{25'}$, located at the Brillouin-zone center. The one-phonon Raman spectrum of silicon, first reported by Russell,[13] and investigated further by Parker *et al.*,[14] and most recently by Chang *et al.*[15] and Hart *et al.*,[16] determined the optical-phonon energy at the Brillouin-zone center to be 519 cm^{-1}. Parker *et al.* also reported the existence of some two-phonon scattering in the 900–1100-cm^{-1} region but made no further use of these two-phonon Raman data to determine phonon energies at other points throughout the Brillouin zone.

The width of the single-phonon peak is a measure of the coupling between the zone-center phonon and other sets of phonons to which it might decay. Half-width measurements of this peak have been made by Russell, and by Parker *et al.*, Chang *et al.*, and Hart *et al.* These measurements were compared to the theoretical linewidths calculated by Cowley[17] and by Klemens.[18]

In this paper we present the one- and two-phonon Raman spectra of silicon. These spectra were interpreted using energy comparison with the inelastic neutron and infrared-absorption data, group-theoretical arguments, and identification of characteristic shapes in the two-phonon Raman spectra with critical points as first suggested by Van Hove.[10] All features other than the single-phonon $\Gamma_{25'}$ peak in the Raman spectrum of silicon must arise from one-phonon processes which, although ordinarily forbidden, occur because of broken translational symmetry or from multiphonon processes. Two-phonon processes, because of the $\vec{k}=\vec{0}$ selection rule, must involve only pairs of phonons having equal magnitude but oppositely directed k vectors. That such pairs always exist is guaranteed by time-reversal symmetry. Three- and four-phonon events also may contribute to the Raman spectrum. However, all features reported in this paper are identified with one- and two-phonon events, and it appears that the Raman cross sections for higher-phonon processes are extremely small.

The wave vector labeling a phonon is called a special k vector if the vector is left unchanged (modulo a reciprocal-lattice vector) by any of the point-group operations (excluding the identify operation) in the space group of the lattice. Those operations which leave the k vector unchanged make up the group of the k vector. For general k vectors the group of the k vector consists of the identity operation only. For the remainder of this paper we will occasionally refer to a phonon labeled by the wave vector k as "the phonon located at k." Lax[19] has shown that, in crystals with an inversion operation in the space group, general-k-vector phonon pairs may participate in the two-phonon Raman process, and that general-k-vector phonon pairs are forbidden to participate in infrared-absorption processes. Of course, the sum of the two k vectors must be zero. Special-k-vec-

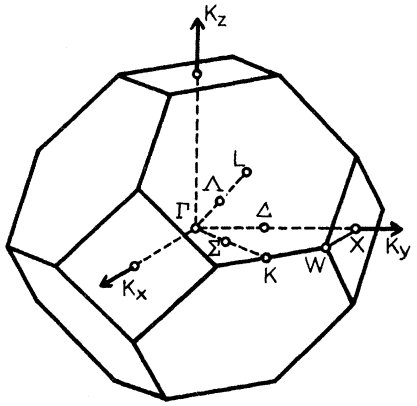

FIG. 2. Brillouin zone for the face-centered space lattice showing the positions of several high-symmetry lines and points.

tor phonon pairs may or may not contribute to two-phonon Raman scattering, depending upon the transformation properties of the pair under consideration.

The two-phonon state is assumed to belong to the product representation (generally reducible) formed from the two representations to which the two phonons belong. The incident and scattered photons belong to the zone-center ($\vec{k}=\vec{0}$) representations. The three representations to which the Raman tensor belongs in this zone-center group are Γ_1, Γ_{12}, $\Gamma_{25'}$. In order to satisfy the selection rule which requires that the net k vector be conserved, the two phonons must have equal but opposite k vectors. Since their net k vector is zero, the product representation for the two-phonon pair consists of a sum of irreducible zone-center representations.

Lax[19] also has shown that, when considering selection rules for space groups, the only group elements which need be used in the selection-rule calculations are the "common group of the wave vector." In this case this is the group of the k vector of the phonons making up the two-phonon pair. Both phonons of the pair belong to the same group but not necessarily to the same representation. In order to derive the selection rules for that pair, one need only use the character table for the small representations for the group of the k vector and, using character products, determine if the two-phonon (reducible-product) representation times the perturbation (Raman tensor) times the ground state (assumed to be Γ_1) contains Γ_1. Since a representation times itself always contains Γ_1, and since the Raman tensor belongs to Γ_1, Γ_{12}, and $\Gamma_{25'}$, this is equivalent to asking if the product representation for the two-phonon state contains Γ_1, Γ_{12}, or $\Gamma_{25'}$.

For symmorphic space groups, the characters for the various "groups of the k vector" are identical to the usual point-group characters. For nonsymmorphic space groups, such as O_h^7, the characters for k vectors interior to the Brillouin zone are the same as for the symmorphic case, that is, the usual point-group characters. However, for k vectors on the surface of the Brillouin zone, the characters may not be the usual point-group characters, and character tables such as those tabulated by Koster[20] must be used. In the event the character vectors are complex, as they are at the point W, it is assumed that the character for the $-k$ phonon is the complex conjugate of the $+k$-phonon character.

Folland and Bassani[21] have tabulated the zone-center-reduction coefficients of the direct-product representations of two-phonon pairs for the symmorphic space group $O_h^5(Fm3m)$. As discussed above, these will be identical to the reduction coefficients for all interior points of the Brillouin zone for nonsymmorphic space groups as well. Therefore, we have used these reduction coefficients when applicable. Even though L lies on the surface of the Brillouin zone, in the diamond structure the character table for the representations at L is identical to the character table at L for the symmorphic space group, and the coefficients listed by Folland and Bassani for L have been used. The character table for W by Koster is incorrect, and the correct table listed by Elliott[22] was used. The group-theoretical selection rules derived in the manner described for two-phonon Raman scattering from general- and special-k-vector phonon pairs for silicon are summarized in Table I.

The shape of the dispersion curve in certain high-symmetry regions of the Brillouin zone is dictated by symmetry requirements. In particular, at the points Γ, L, X, and W all of the components of the gradient of the energy in k space are required to be zero. Phillips[11,12] has labeled these critical points P_j according to the number of principal directions j in k space in which ω decreases from its value ω_0 at the critical point. The density-of-states curve will exhibit a well-defined shape behavior for phonon energies near the critical-point phonon energies. The shapes of critical-point contributions to the density-of-states curve, as discussed by Phillips and by Johnson and Loudon,[6] are shown in Fig. 3. The assignments of critical-point types P_j are indicated in Table II.

Since all general $\pm k$ phonon pairs may contrib-

TABLE I. Group-theoretical selection rules for two-phonon Raman and infrared activity for the diamond structure. The notation is that used by Bouckaert, Smoluchowski, and Wigner (Ref. 34).

Region in k space	One-phonon representations	Zone-center reduction coefficients Γ_1	Γ_{12}	$\Gamma_{25'}$	Γ_{15}
General point		1	1	1	0
Γ	$\Gamma_{25'}\otimes\Gamma_{25'}$	1	1	1	0
X	$X_1\otimes X_1$, $X_2\otimes X_2$	1	1	1	1
	$X_3\otimes X_3$, $X_4\otimes X_4$	1	1	1	0
	$X_1\otimes X_2$	0	1	0	0
	$X_1\otimes X_3$, $X_1\otimes X_4$, $X_2\otimes X_3$, $X_2\otimes X_4$	0	0	1	1
	$X_3\otimes X_4$	0	1	0	1
L	$L_1\otimes L_1$, $L_{2'}\otimes L_{2'}$	1	0	1	0
	$L_3\otimes L_3$, $L_{3'}\otimes L_{3'}$	1	1	2	0
	$L_1\otimes L_{2'}$	0	0	0	1
	$L_1\otimes L_3$	0	1	1	0
	$L_1\otimes L_{3'}$	0	0	0	1
	$L_2\otimes L_3$	0	0	0	1
	$L_{2'}\otimes L_{3'}$	0	1	1	0
	$L_3\otimes L_{3'}$	0	0	0	2
W	$W_1\otimes W_1$, $W_2\otimes W_2$	1	1	1	1
	$W_1\otimes W_2$	0	1	2	2
Σ	$\Sigma_1\otimes\Sigma_1$, $\Sigma_2\otimes\Sigma_2$, $\Sigma_3\otimes\Sigma_3$, $\Sigma_4\otimes\Sigma_4$	1	1	1	1
	$\Sigma_1\otimes\Sigma_2$, $\Sigma_3\otimes\Sigma_4$	0	0	1	0
	$\Sigma_1\otimes\Sigma_3$, $\Sigma_2\otimes\Sigma_4$	0	0	1	1
	$\Sigma_1\otimes\Sigma_4$, $\Sigma_2\otimes\Sigma_3$	0	1	0	1

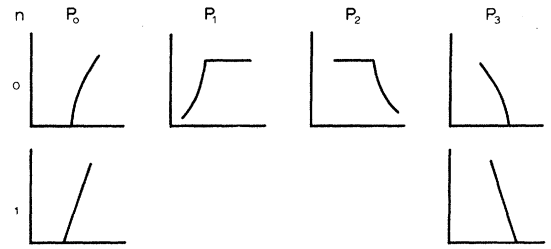

FIG. 3. Shapes of critical-point contributions to the density of states. The critical-point designation, P_j and F_j, is that of Phillips (Ref. 11) and of Johnson and Loudon (Ref. 6). The number n refers to the number of principal directions in which the phonon branch has a discontinuous first derivative.

ute to the two-phonon Raman process, as contrasted with the two-phonon infrared-absorption process, and since the shapes displayed in Fig. 3 consist of contributions from general-k-vector phonons in the neighborhood of the critical phonon as well as those special-k-vector phonons at the critical point, one would expect the two-phonon Raman spectrum to reflect clearly the density of states and therefore, in the case of overtones, the shapes displayed in Fig. 3. The shapes of the various features in the Raman spectra were helpful in identifying the branches and critical points contributing to these features.

EXPERIMENTAL

All spectra for this paper were obtained using an argon-ion laser[23] tuned to 488.0 nm as the excitation source. That these spectra were actually Raman scattering was confirmed by using the 514.5-nm line as the excitation wavelength. Laser power varied from 1.2 W to 800 mW during the course of the experiment. A Spex model-1401 double monochromator using a Jarrell-Ash grating with 1180 lines per mm was used in conjunction with an ITT FW-130 photomultiplier. The response of the instrument was determined using an Electro-Optics Associates P101 standard lamp as a source.

A laser-power-monitor system was used in order to overcome any short- or long-term fluctuations in signal output introduced by laser-power fluctuations.[24] The photomultiplier-signal pulses were counted until the laser-power monitor indicated that a given laser-photon fluence was incident upon the sample. At that time the number of photomultiplier-signal pulses gathered during that counting interval was printed and the spectrometer setting was stepped to the next spectral position. The process was then repeated. By defining the spectral-counting interval in this way, we were assured that each data point represented a relative scattering cross section for that wavelength normalized to a given incident photon fluence. Unless otherwise noted, the data presented in this paper were gathered with 4-cm^{-1} spectral slit width, and 1-cm^{-1} spectral increments. The counting times per spectral position based on a laser power of 900 mW varied from 40 sec for the survey scans to 100 sec for the detailed spectra. The exact time per interval depended upon the laser power as discussed above. The data gathered were then corrected for the instrument response and plotted as individual points. We have retained the "as-gathered" digital form of the data in the figures in order to indicate the relative uncertainties involved. It should be noted that, even though these data are digital, the number assigned to each spectral position is a measure of the energy and not the number of photons scattered into that spectral interval. This is because the throughput was determined by using a lamp with a known spectral power output. The number of photons scattered into a spectral interval is proportional to the product of photon wavelength and the intensity we assign to that spectral interval.

The silicon sample was mounted in a "cryo-tip" Dewar.[25] This allowed data to be gathered at temperatures between 305 and 17 °K. The sample configuration which allowed 180° Raman scattering to be collected is shown in the upper-right-hand corner of Fig. 4. The laser beam passed through the mirror, was spectrally reflected from the silicon sample, and passed back through the hole in the mirror. The scattered radiation was reflected from the mirror, passed through the lens system, and entered the spectrometer. In this sample arrangement the incident and scattered electric field vectors lie in the plane of the sample surface. Since the incident beam is normal to the surface of the sample, changing the incident and scattered polarization directions has no effect on the percentage of incident laser light being absorbed by the sample. In the typical 90° scattering configuration with silicon, as indicated in Fig. 11, this is not the case, and changes in incident

TABLE II. Phonon critical-point assignments.

Branch[b]	Critical-point location[a] Γ	X	L	W	Σ
TO 1	P_3	P_0	P_2	P_1	P_2P_1
TO 2	P_3	P_0	P_2	P_3	P_2P_1
LO	P_3	P_2	P_2	P_0	P_1
LA	P_0	P_3	P_1	P_2	...
TA 1	P_0	P_1	P_1	P_1	P_3
TA 2	P_0	F_2	P_1	P_3	...

[a]The notation is that of Phillips (Ref. 11) and Johnson and Loudon (Ref. 6). F_2 refers to a fluted saddle point. The shapes associated with the various P_j critical points are shown in Fig. 2.

[b]The branches are labeled in decreasing energy.

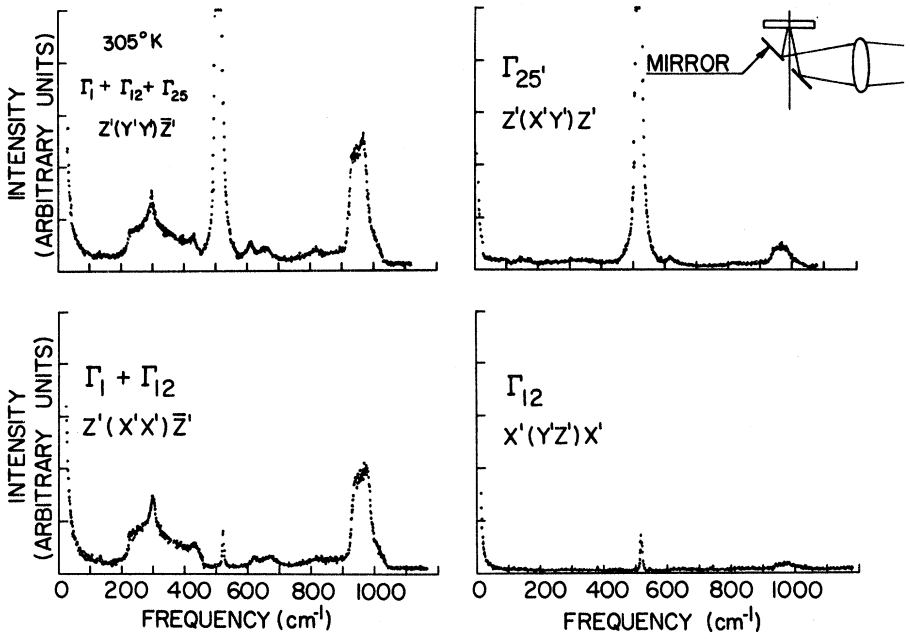

FIG. 4. The Raman spectrum of silicon at room temperature. The spectra were all measured using 4 cm^{-1} slits. The data points are 1 cm^{-1} apart. The polarization configuration and the representations which were possible contributors to the spectra are shown for each of the four spectra. The spectra have been corrected for instrumental throughput.

polarization direction strongly affect the percentage of laser light absorbed and, therefore, the strength of the Raman signal detected. In the 90° configuration, the greatest absorption, and therefore the strongest Raman scattering, is observed with the incident laser light polarized so that the electric field vector points into the surface, and the least Raman scattering is observed when the electric field vector of the incident light is parallel to the surface of the silicon sample. Because of these difficulties, as well as the high index of refraction of silicon in the visible, it is not possible to use the 90° configuration to make quantitative measurements of the Raman scattering-tensor elements. The data gathered using the configuration shown in Fig. 4, however, need only be corrected for differences in reflectivity of the small front-surface mirror for the two reflected polarizations. It should be noted, however, that for the backward (180°) scattering configuration the resultant phonon excitation must have twice the k vector of the incident photon. While the k vector associated with this phonon excitation is not zero, it is displaced from the $k=0$ axis at most 0.2% of the maximum value of a k vector at the zone edge.

Figure 5 shows two coordinate systems fixed in the silicon sample. The unprimed coordinates correspond to the usual cube edges. The primed coordinates correspond to a system rotated about the [100] axis by 45°. If incident- and scattered-photon polarization directions are chosen to be parallel to the primed (or unprimed) axes, then the Raman-scattered intensity will be proportional to the square of only one element in the scattering tensors when the tensor is expressed in the primed (or unprimed) coordinate system. If arbitrary polarization directions had been chosen, the intensity would generally contain a sum of terms which included several of the scattering-tensor elements. In the case of two- and three-fold degenerate representations, the intensity will be proportional to the sum of the squares of the appropriate element from each of the two or three scattering tensors for that representation. Figure 5 shows two sets of matrices for the three representations to which

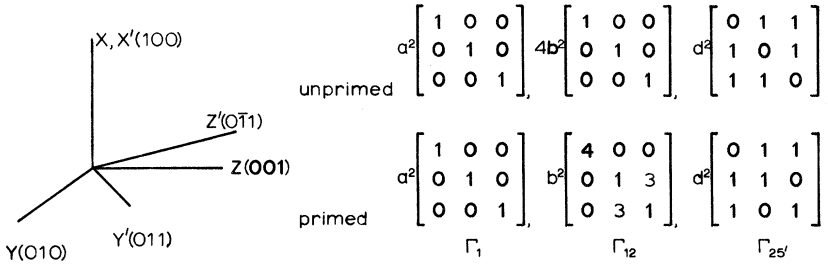

FIG. 5. The two sets of Raman intensity matrices for the three representations to which the polarizability tensor belongs in the cubic point group. The two sets of axes long which the incident and scattered polarization vectors are aligned are also shown. The derivation and use of these matrices is discussed in the text.

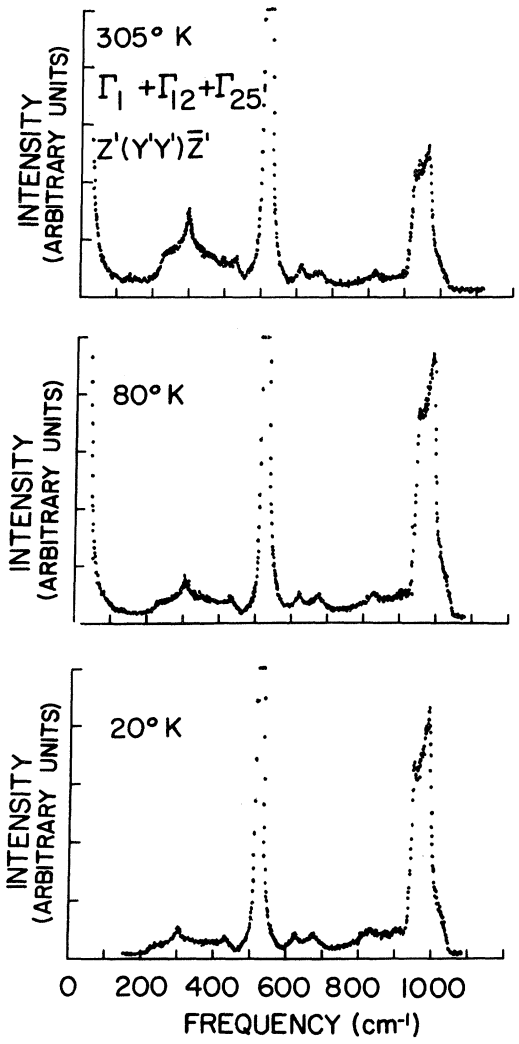

FIG. 6. The Raman spectra of silicon measured at 305, 80, and at 20 °K. The experimental parameters are identical to those in Fig. 4.

the polarizability tensor belongs in the O_h point group.[26] The elements of the matrices are the square of the corresponding scattering-tensor elements. For the two- and three-fold representations, the matrix element shown is the sum of the squares of the appropriate tensor elements. The primed and unprimed intensity matrixes shown in Fig. 5 correspond to having the polarization directions either parallel to the primed or parallel to the unprimed coordinate system. When the intensity matrices for Raman scattering are shown in this way, it is quite easy to determine the Raman-scattering polarization characteristics for phonons belonging to the three representations.

Figure 5 shows that the choice of a sample with [100] face allows the unique determination of the transformation characteristics of all Raman-scattered radiation. The eight elements which can be measured with a [100]-face sample are YY, YZ, ZY, and ZZ using the unprimed axes, and $Y'Y'$, $Y'Z'$, $Z'Y'$, and $Z'Z'$ using polarization directions parallel to the primed set of axes. The only off-diagonal element in the unprimed configuration belongs to the $\Gamma_{25'}$ representation, and the only off-diagonal element in the primed coordinate configuration belongs to the Γ_{12} representation. It was therefore possible to uniquely determine the presence of scattering belonging to these two representations. By comparison of diagonal and off-diagonal intensities it was possible to determine the presence of Γ_1 scattering.

A second method for determining the transformation characteristics of the Raman-scattered radiation involved the use of two samples, one with [100] face and a second one with $[0\bar{1}1]$ face. Using the [100] sample, the four intensity matrix elements measured were $Y'Y'$, $Y'Z'$, $Z'Y'$, and $Z'Z'$, as above. The $[0\bar{1}1]$ face sample allowed the measurement of $X'X'$, $X'Y'$, $Y'X'$, and $Y'Y'$ intensity matrix elements. Again, the only off-diagonal intensity matrix elements belong to Γ_{12} and $\Gamma_{25'}$ representations and the presence of Γ_1 scattering was determined by comparison of diagonal and off-diagonal intensities. Figure 4 shows the Raman spectra obtained by using two samples. The spectra have been labeled both according to representation and the experimental configuration under which the data were obtained. The $Z'(Y'Y')\bar{Z}'$ spectrum was used as a general survey spectrum because all three representations are allowed to contribute to the scattering.

The samples were obtained from Dow Corning Corporation.[27] The samples were two-pass vacuum zone refined and were stated to contain less than 400-ppb carbon, less than 50-ppb oxygen, less than 0.01 ppb other heavy metals, and approximately 0.15-ppb boron and 0.05-ppb phosphorus. The resistivity of all samples was approximately 3000 Ω cm. All samples were p type. The samples were oriented by Laue back reflection to within 1° of stated orientation and were mechanically polished by Dow Corning. We further polished these samples with Monsanto Syton HS, a commercial chemical-mechanical polish, to remove all surface damage. The samples were attached to the "cryo-tip" with a heat-conductive grease. The temperature of the sample was measured by a thermocouple mounted very near the sample end of the high-purity-copper cryostat tip.

Figure 4 shows the polarization data obtained for silicon at 305 °K. The polarization characteristics of all one- and two-phonon Raman features are shown in this figure. Figure 6 shows the same polarization data, $Z'(Y'Y')\bar{Z}'$, measured at 305, 80, and 20 °K. The intensity scales for the three spec-

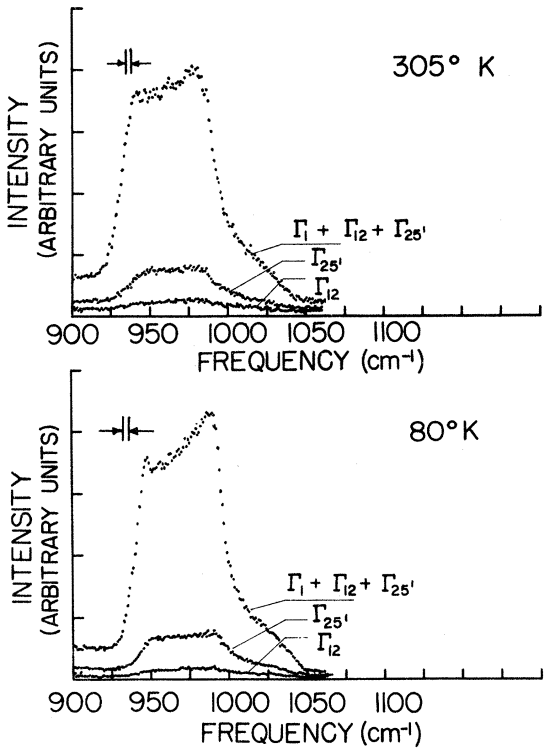

FIG. 7. Detail of the Raman spectrum of silicon in the 900–1110 cm^{-1} region. The representations to which the contributing phonon pairs belong are indicated along with the temperature and the instrumental slit width of 4 cm^{-1}. The spectrum is the sum of several identical spectra. The data points are 1 cm^{-1} apart. The spectra have been corrected for instrumental throughput.

TABLE III. Half-widths of the zone-center Raman-active phonon.

Temperature	Half-width (cm^{-1}) Approximate measurement from raw data	Deconvoluted
17 °K	1.6	1.45±0.05
30 °K	1.6	1.45±0.05
80 °K	1.9	1.80±0.05
305 °K	3.6	3.50±0.05

tra shown in Fig. 6 are identical. Figure 7 is a detail of the region from 900–1100 cm^{-1} measured at 305 and 80 °K and indicates the polarization characteristics and spectral shape of this region in greater detail. Figure 8 shows the detail of the region from 0–500 cm^{-1}. Figure 9 shows the one-phonon line at Γ, the zone center, measured at 17, 30, 80, and 305 °K using $\frac{1}{2}$-cm^{-1} spectral slit widths and 0.1-cm^{-1} spectral steps. A spectrum of the laser line (488.0 nm) using the same spectrometer settings is included for comparison. The half-widths indicated on Fig. 9 are uncorrected for the finite instrument slit width. The deconvoluted half-widths are shown in Table III.[28] The observed phonon energies associated with the various regions throughout the Brillouin zone are summarized as determined from all the measurements made in Table III. Inelastic-neutron and infrared-absorption data are also indicated in this table.

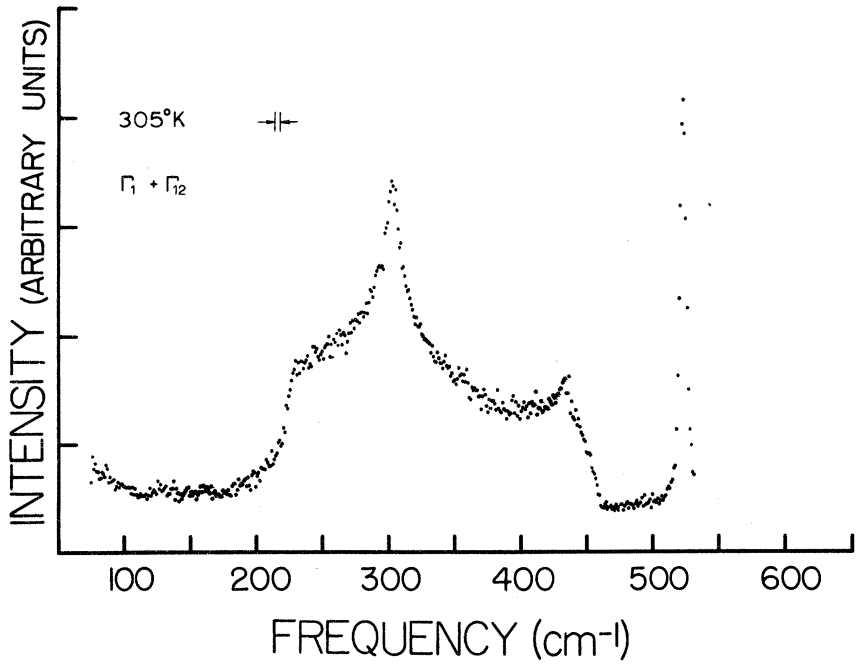

FIG. 8. Detail of the spectrum of silicon in the 0–500 cm^{-1} region. The representations to which the contributing phonon pairs belong are indicated along with the temperature and instrumental slit width of 4 cm^{-1}. The spectrum is the sum of several identical spectra. The data points are 1 cm^{-1} apart. The spectrum has been corrected for instrumental throughput.

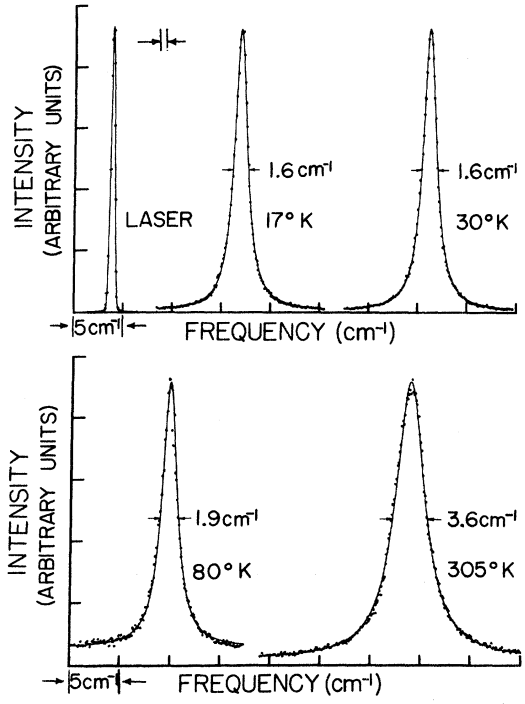

FIG. 9. The one-phonon Raman line in silicon measured at several temperatures. The data have all fitted to Lorentzian curves. The laser line, which has been fit to a Gaussian, is also shown. The spectral slit width was $\frac{1}{2}$ cm^{-1} for all spectra. The data points are 0.1 cm^{-1} apart and are shown as gathered. The half-width is indicated on each spectrum.

DISCUSSION OF RESULTS

While prominent features in the two-phonon spectra are associated with critical points which are either accidental or required by symmetry, the bulk of the scattering associated with that critical point will be made up of scattering from two-phonon pairs which lie near the critical-point phonon. That Raman scattering can occur in the diamond structure for two-phonon pairs when these phonons are labeled by general k vectors has been discussed above. The two-phonon pair for general k vectors transforms according to all representations of Γ. The reducible representations of the two-phonon pair will therefore contain Γ_1, Γ_{12}, and $\Gamma_{25'}$ symmetry. Thus, all spectra might contain contributions from general-k-vector phonon pairs.

There is the possibility that an accidental critical point will occur which involves only general-k-vector phonons. As pointed out by Dolling and Cowley,[9] the calculated density of states for silicon contains regions of high density which cannot be identified with features on the neutron dispersion curve and might therefore be identified with accidental critical points. Figure 10 is a superposition of the calculated density of states[9] and the two-phonon Raman-scattering data. Such a region appears at 670 cm^{-1} (10.1×10^{12} Hz) in Fig. 10. That there is a corresponding feature in the two-phonon Raman spectrum can be seen in Figs. 4, 6, and 10. This feature has Γ_1 symmetry only.

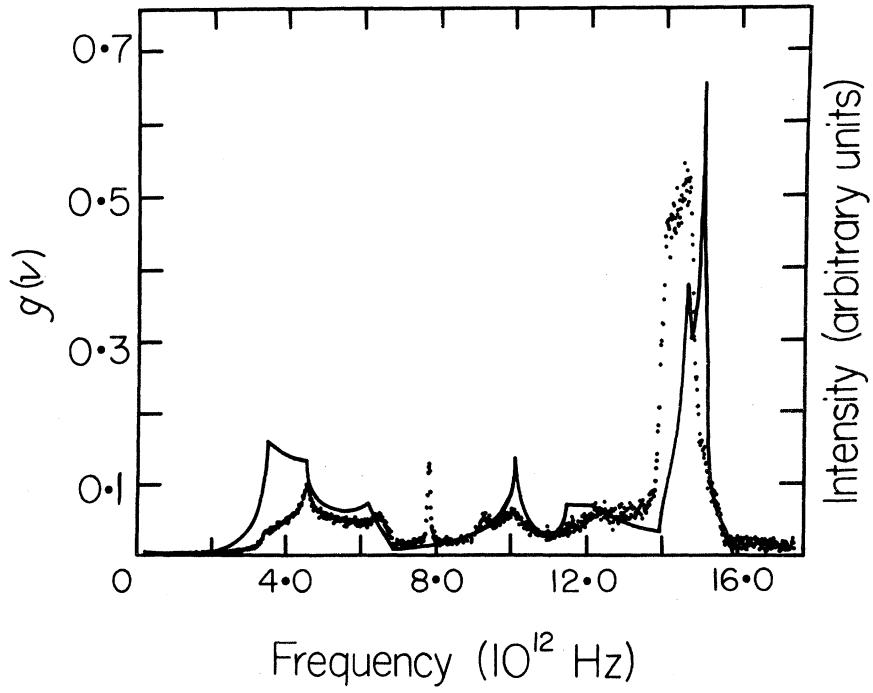

FIG. 10. The superposition of the density of states calculated by Dolling and Cowley (Ref. 9) and our two-phonon Raman data as measured at 305 °K and modified as discussed in the text.

TABLE IV. Phonon frequencies at the critical points.

Critical points		Phonon frequencies (cm^{-1}) Infrared *J* and *L* (Ref. 6)	Infrared *B* and *N* (Ref. 7)	Neutron (Ref. 1)	Present Raman
Γ	0	522	517 ± 2	518 ± 3	519 ± 1
X	TO	463	449 ± 3	464 ± 10	460 ± 2
	TA	149	155 ± 5	150 ± 2	151 ± 2
L	TO	491	493 ± 2	490 ± 10	490 ± 2
	TA	114	113 ± 2	114 ± 2	113 ± 2
W	TO		478 ± 13	481 ± 13	470 ± 2

The feature at 610 cm^{-1} in the two-phonon Raman data is associated with a combination of acoustic and optic phonons in the Σ direction. This scattering exhibits both Γ_1 and $\Gamma_{25'}$ symmetry. This is the only combination observed in the two-phonon Raman data, with all other features being associated with overtones. This assignment has been made on energy considerations and group-theoretical exclusion of other possible combinations.

The polarization characteristics of the remaining structure in Fig. 4 will be discussed next. Table I indicates that Γ_{12}-type scattering is allowed in several situations involving high-symmetry k-vector phonons as well as general-k-vector phonons. Figure 4 shows that there is very little, if any, scattering of this type. The only Γ_{12} scattering is in the 900–1100-cm^{-1} region, and the intensity there is quite weak. This is best seen in Fig. 7. Certainly there are no significant features in the Γ_{12} spectrum. However, the lack of Γ_{12} scattering is not a violation of group-theoretical selection rules.

The most intense feature in the $\Gamma_{25'}$ data in Fig. 4 is the one-phonon peak at 519 cm^{-1}. The intensity as gauged by peak height of the single-phonon scattering is greater than the strongest second-order scattering by a factor of 35. This feature is highly polarized, with a polarization ratio of 100:1. It should be noted that this is the instrumental limit of a polarization measurement. This one-phonon line is therefore a convenient check on the reliability of the polarization data in general.

Figure 8 has been included to show the measured half-width and Lorentzian nature of the zone-center one-phonon peak. These raw data have been fitted to Lorentzian line shapes. The uncorrected data indicate that the width at half-maximum intensity which we have measured is about 25% less than that extrapolated by Hart *et al.*[16] This uncorrected half-width agrees very well with the value reported by Chang *et al.*[15] using a Nd-YAG laser. Table III lists the half-width of silicon for several temperatures between 17 and 305 °K as recorded. The half-widths extracted by deconvolution with the measured laser line shape and determined under the same experimental conditions are also listed.

It is clear that our measured half-widths are definitely smaller than those reported by Hart *et al.* In this experimental arrangement, the laser intensity reaches an intensity of $(1/e)$ at a depth of approximately 10 000 Å. While this depth is well below the surface, certainly the surface could play a significant role in the decay processes which are reflected in the half-width of this phonon. It is possible that the surface of web-grown silicon as used by Hart *et al.* is sufficiently different from our polished surface to cause this difference. The measurement made by Chang *et al.* using a Nd-YAG laser, whose energy is below the electronic band gap, is a bulk-property measurement while the measurements made by Argon laser excitation appear to be much more sensitive to surface condition. Also, it is possible the impurity level in the sample used by Hart *et al.* was higher than in the sample measured in this experiment. Parker *et al.* indicated an increased linewidth with doping when they measured the half-width of the one-phonon line in silicon.

That the zone-center one-phonon line is very nearly Lorentzian can be seen in Fig. 9. Since this method of Raman scattering allows one to sample this phonon as far away from $k = 0$ as is possible for the creation of a single phonon, one might expect a wider and non-Lorentzian line. The phonon is triply degenerate at $k = 0$, but the degeneracy is lowered for $k > 0$. The lowering of the degeneracy for $k > 0$ is not evident in the optical-phonon line shape as measured in this experiment. The laser line as fitted by a Gaussian curve is also shown in Fig. 9 to indicate its possible contribution to the silicon line shape and width. Both measured and deconvoluted half-widths are indicated in Table III.

The scattering at 610 cm^{-1} in the $\Gamma_{25'}$ spectrum has been discussed above. The scattering in the 900–1050 cm^{-1} region, most easily seen in Fig. 7, may be associated with overtones and combinations involving optical phonons which lie throughout the Brillouin zone. The sharp increase in the $\Gamma_{25'}$ spectrum at 920 cm^{-1} (930 cm^{-1} at 80 °K) is identified with the two TO-phonon overtone scattering from the critical point at *X*. The shoulder at 940 cm^{-1} (950 cm^{-1} at 80 °K) is identified with the two TO-phonon overtone at *W*. Phonon energies at *W* were not measured by Dolling.[1] Balkanski and Nusimovici[7] have assigned the value of 965 cm^{-1} to the phonon at *W*. The shape of this shoulder, which corresponds to a critical point of type P_1, indicates that this assignment is correct. The shoulder at 975 cm^{-1} (985 cm^{-1} at 80 °K), which exhibits critical-point character of type P_2, is identified with the two TO-phonon overtone scattering from the critical point at *L*.

The optical-phonon energy reaches a maximum at the zone center. The triple degeneracy of the optical phonon at this point requires the density of

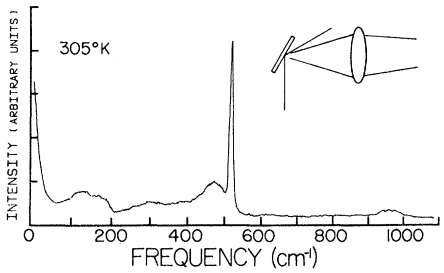

FIG. 11. The 305 °K Raman spectrum of silicon which has been damaged by the implantation of 60 keV phosphorous ions. The experimental configuration is indicated in the upper right corner.

states to have the form of the critical point P_3. The termination of the two-phonon scattering at 1040 cm^{-1} (1050 cm^{-1} at 80 °K) is associated with the rapid decrease in the density of states at this critical point. No scattering has been detected above 1040 cm^{-1} except for some extremely weak-scattered radiation in the neighborhood of 1500 cm^{-1}. This can be attributed to three-phonon processes associated with the high density of phonon states at approximately 500 cm^{-1}. No "bound-phonon pairs" were observed in silicon. The existence of such bound-phonon pairs in diamond has been suggested by Ruvalds[29] in order to explain the unexpected peak at more than twice the zone-center phonon energy in the diamond two-phonon Raman data.[8]

With all the features listed above, the shapes of the critical-point contributions to the density of states, and therefore the two-phonon Raman spectra, agree with the assignments of Phillips and of Johnson and Loudon. While it is possible there are two-phonon combinations contributing to the scattering in the 900–1050 cm^{-1} region, no prominent features associated with combinations are apparent.

The very weak scattering observed in the vicinity of 150 cm^{-1} in the $\Gamma_{25'}$ spectrum is associated with one-phonon Raman scattering from acoustic phonons which are not at the zone center. Such "forbidden" first-order scattering is allowed when the perfect translational symmetry of the crystal is disrupted. Pure silicon consists of about 92% Si^{28}, 5% Si^{29}, and 3% Si^{30}. This mass difference, along with other imperfections, evidently is sufficient to allow a small amount of one-phonon Raman scattering for nonzero k-vector phonons. In support of this statement, Fig. 11 shows a spectrum taken at room temperature of a [111]-surface silicon wafer which has been damaged by the implantation of phosphorus ions to a local density of approximately 10^{20} per cm^3. The implantation energy was 60 keV. This energy placed the bulk of the phosphorus ions and damage between the surface and approximately 700 Å into the sample, a region strongly sampled by the laser beam. This spectrum demonstrates the nature of Raman scattering from damaged silicon and is used to contrast the spectrum of damaged silicon with two-phonon Raman spectrum of undamaged silicon. This spectrum was obtained in the usual 90° scattering configuration also shown in Fig. 11. The polarizer and analyzer were parallel, allowing both Γ_1 and $\Gamma_{25'}$ scattering. There are several significant features in the spectrum shown in Fig. 11. The presence of the band of scattering beginning near the laser line and ending at about 200 cm^{-1} corresponds to the region noted above in the $\Gamma_{25'}$ spectrum of Fig. 4. The region of strong scattering just below the energy of the one-phonon peak at 519 cm^{-1} corresponds to a region of high density of states in undamaged silicon. The intensity of the two-phonon structure in the 900–1050 cm^{-1} region is much lower than the scattering intensity in the 150 cm^{-1} region. This is in direct contrast to the $\Gamma_{25'}$ data of Fig. 4. Data on amorphous silicon, similar to Fig. 11 but not showing the presence of the one-phonon peak at 519 cm^{-1} and the structure at 900–1050 cm^{-1}, was reported by Smith *et al.*[30] As noted by Smith, there is a similarity between the density of states in undamaged silicon and the Raman spectrum of damaged or amorphous silicon.

The Γ_1 spectrum in Fig. 4 shows the most intense scattering. Nearly all the scattering between 0 and 500 cm^{-1} is Γ_1. Details of this region are shown in Fig. 8. This region consists of overtones of acousitc phonons only. As indicated in Table IV the kink at 230 cm^{-1} is associated with the TA phonon at L. The peak at 302 cm^{-1} is associated with the TA phonon at X, and the peak at 435 cm^{-1} and the termination of scattering at 460 cm^{-1} is associated with scattering involving phonons along and near Σ. All these assignments are consistent with the critical-point contributions to the shape of the density of states as shown in Fig. 3 and Table II. The feature at 670 cm^{-1} has been discussed above. The features in the 900–1050-cm^{-1} region have been discussed under the $\Gamma_{25'}$ data.

It is not possible to measure the temperature dependence of the one- and two-phonon scattering cross section in silicon in the same manner as one would for an insulator when using an exciting source with photon energy greater than the energy of the electronic band gap of silicon. Because of the 1.1-eV band gap and the 2.5-eV laser photon energy, there are photon-absorption processes which may be temperature dependent and may be competing with the Raman process. The number of photons available to participate in the Raman process is dependent upon these competing processes. In effect, the Raman process is screened by absorption of both exciting photons and Raman-scattered pho-

tons. It is possible, however, to draw some conclusions concerning the temperature dependence of the Raman process.

Because of absorption of photons, it is clear that the measured Raman intensity will be dependent upon the value of the absorption coefficient. That the absorption coefficient varies with temperature is indicated by the data of Dash *et al.*[31] Their data indicate that the absorption coefficient for silicon decreases by a factor of approximately 2 in going from room temperature to 80 °K for a 2.5 eV photon. One would expect an increase in Raman scattering intensity at 80 °K over the 305 °K scattering intensity due to this lessened absorption, and this in fact appears to be the case.

In addition to the temperature dependence introducted by the absorption coefficient, as discussed above, the one-phonon Stokes process should exhibit an $(n+1)$ temperature dependence, and the two-phonon-overtone process should exhibit an $(n+1)^2$ temperature dependence owing to population dependence in the scattering intensity. The Bose–Einstein population factor is denoted by n. In addition, there might be temperature dependence in the matrix elements connecting the electric field to the electronic and phonon states. The photon energy of 2.5 eV is well outside the resonance Raman energy region, and no strong temperature dependence due to electronic band shifts are expected as was the case in the measurements of Chang *et al.*

In order to remove the effect of competing absorption processes on the intensity, we have assumed in the following discussion that the temperature dependence of the matrix elements for one-phonon Raman scattering is small. For the one-phonon 519-cm^{-1} line, the ratio $(n+1)_{305\,°K}/(n+1)_{80\,°K}$ is 1.09, while the measured intensity ratio is 1.88. We have assumed that this difference is due only to absorption processes competing with the Raman effect as discussed above. If now the 305 °K spectra are adjusted by multiplying the two-phonon intensity by the factor 2.05, we find that the ratios of intensity of two-phonon overtone features at 305 °K to their intensity at 80 °K exhibit the expected population dependence on temperature. This is displayed in Table V.

In Table V the measured ratios of intensity at 305 °K to intensity at 80 °K times the factor 2.05 for various regions in the two-phonon Raman spectrum are listed. Also listed is the calculated value of $(n+1)^2_{305\,°K}/(n+1)^2_{80\,°K}$ for the same phonon energies. To measure the one-phonon intensity as well as the two-phonon intensity, slits of 10 cm^{-1} width were used. This slit width allowed nearly all the one-phonon line to enter the spectrometer with the spectrometer centered on the one-phonon frequency. For the two-phonon spectra, relatively flat regions of the spectrum were chosen in order to eliminate the possibility of peak-position shifts with temperature which would cause anomalous intensity changes not related to the intended measurement. Also, the spectral positions measured were shifted upward for the 80 °K measurements in order to include the upward shift in phonon energy with decreasing temperature. As was done in the case of the one-phonon line, the spectrometer was centered on the region indicated and was not scanned. The spectral positions measured are indicated in Table V. The data in Table V are the average of five 305 °K and 80 °K data runs. The ratio of these intensities are accurate to about 8%. Mechanical stability of the sample position with respect to the laser and monochromator limited the accuracy of this measurement.

The data in Table V indicate that the two-phonon Raman spectrum, after being modified by the one-phonon intensity ratio, displayed to within experimental error the usual $(n+1)^2$ temperature dependence. The apparent increase in scattering intensity in the 900–1050 cm^{-1} region seen in Fig. 6 is evidently due to decreased screening because of the smaller absorption coefficient at 80 °K than at 305 °K. While we initially assumed that the one-phonon matrix element was temperature independent, the analysis we have used allows for the possibility that any temperature dependence which is present in the one-phonon matrix element may also be present in the two-phonon matrix element.

Figure 10 is a superposition of our two-phonon Raman data and Dolling and Cowley's calculated one-phonon density of states for silicon. The Raman spectrum shown in this figure is the $\Gamma_1+\Gamma_{12}$ spectrum obtained at 305 °K. This symmetry configuration eliminates all but about 1% of the one-phonon line at 519 cm^{-1}. The Raman data have been modified in the following way. Each datum point shown on the figure has been divided by the factor $(n+1)^2_{305\,°K}$, where n has been calculated for the frequency corresponding to one-half the frequency of the datum point. Also, the horizontal scale has been reduced by a factor of 2 in order to show the correspondence between the one-phonon density of states and the two-phonon Raman data. The vertical scale of the Raman data has been adjusted to

TABLE V. Measured and calculated intensity ratios at 305 and 80 °K.

Raman frequency (cm^{-1})	$(I_{305\,°K}/I_{80\,°K})(2.05)$	$\frac{(n_\nu+1)^2_{305\,°K}}{(n_\nu+1)^2_{80\,°K}}$
240	4.28	4.18
300	3.77	3.38
400	3.04	2.53
975	1.25	1.23

give a convenient height for comparison with the calculated density of states. As noted in the Introduction the two-phonon Raman spectrum should show a strong correspondence to the density of states. The two-phonon overtone density of states has the same shape as the one-phonon density of states. The only two-phonon combination is the feature at 9.4×10^{12} Hz (610 cm^{-1}). All other possible combinations evidently have extremely small Raman cross sections.

The above adjustments for population dependence in the intensity have been made in order to indicate more clearly the two-phonon Raman cross section as a function of frequency. The modified spectrum shown in Fig. 10 is quite similar to the low temperature spectra shown in Fig. 6. This is consistent with the discussion above concerning the $(n+1)^2$ temperature dependence of two-phonon Stokes scattering.

Several features of Fig. 10 are of interest. The kinks at 3.4×10^{12} and 4.5×10^{12} Hz correspond to the TA phonons at L and X. The rapid falloff of Raman intensity for lower energies indicates that low-frequency acoustic phonon pairs evidently have a small Raman cross section. The peak at 6.5×10^{12} Hz agrees well with the Raman data. The small peak at 9.4×10^{12} Hz is a two-phonon combination, and the one-phonon density of states will not show this feature. The feature at 10.1×10^{12} Hz evidently corresponds to a general region in the Brillouin zone where an accidental critical point occurs. The energy for the phonon at W is 10.7×10^{12} Hz, somewhat higher than this value, and this feature, therefore, does not correspond to the phonon at W.[32] The region from 11.0×10^{12} to 14.0×10^{12} Hz in the Raman spectrum shows less similarity to the density of states than does the lower-energy region.

The region from 14×10^{12} to 16×10^{12} Hz is of particular interest. The positions of the sharp increases in density of states and in Raman scattering agree quite well. Also, the termination of scattering and of states at the zone center are in agreement as previously discussed. However, the peak in Raman scattering at 14.1×10^{12} Hz, which we have assigned to the TO phonon at W, does not appear in the density-of-states calculation. The peak at 14.6×10^{12} Hz is assigned to the TO phonon at L and is in agreement with the density-of-states assignment. The large peak at 15.1×10^{12} Hz in the calculated density of states does not appear in the Raman spectrum. The origin of this feature appears to be states on and near the optical branch in the Σ direction. The fitted curve for this branch in Fig. 1, the dispersion curve, is consistently higher than the neutron data, and it appears as though this spike in the density of states is a result of the model used to describe the dispersion of silicon.

The shift in frequency of the two-phonon overtones from exactly twice the one-phonon frequencies, which has been suggested by Dolling and Cowley, has not been observed. In particular, the termination of Raman scattering at exactly twice the zone-center phonon frequency demonstrates this statement.

SUMMARY

The one- and two-phonon Raman spectra of silicon have been measured as a function of temperature. Several of the critical-point phonon energies have been deduced from the polarization data by use of the critical-point contributions to the shape of the density-of-states curve, neutron scattering data, and group-theoretical arguments. The intensity of the two-phonon spectrum has been shown to include the expected $(n+1)^2$ temperature dependence. The one-phonon line shape has been shown to be Lorentzian and to have a linewidth of 1.45 ± 0.05 cm^{-1} at 17 °K.

ACKNOWLEDGMENTS

We wish to thank N. O. Folland and G. Dolling for their helpful and critical discussions. In addition, we wish to thank Dr. Leon Crossman of Dow Corning Corporation for assistance in obtaining the needed silicon samples.

---

*Supported in part by the Office of Naval Research, Contract No. N00014-68-A-0504.

†Present Address: Northwest Missouri State University, Maryville, Missouri 64468.

[1]G. Dolling, in *Inelastic Scattering of Neutrons in Solids and Liquids*. (International Atomic Energy Agency, Vienna, 1963), Vol. II, p. 37.

[2]B. N. Brockhouse and P. K. Iyengar, Phys. Rev. 111, 747 (1958).

[3]J. L. Warren, J. L. Yarnell, G. Dolling, and R. A. Cowley, Phys. Rev. 158, 805 (1967).

[4]B. N. Brockhouse and B. A. Dasannacharya, Solid State Commun. 1, 205 (1963).

[5]F. A. Johnson, Proc. Phys. Soc. 73, 265 (1959).

[6]F. A. Johnson and R. Loudon, Proc. Roy. Soc. A 281, 274 (1964).

[7]M. Balkanski and M. Nusimovici, Phys. Stat. Sol. 5, 635 (1964).

[8]S. A. Solin and A. K. Ramdas, Phys. Rev. B 1, 1687 (1970).

[9]G. Dolling and R. A. Cowley, Proc. Phys. Soc. 88, 463 (1966).

[10]L. Van Hove, Phys. Rev. 89, 1189 (1953).

[11]J. C. Phillips, Phys. Rev. 104, 1263 (1956).

[12]J. C. Phillips, Phys. Rev. 113, 147 (1959).

[13]J. P. Russell, J. Phys. Radium 26, 620 (1965).

[14]J. H. Parker, Jr., D. W. Feldman, and M. Ashkin, Phys. Rev. 155, 712 (1967).

[15]R. K. Chang, J. M. Ralston, and D. E. Keating, in *Light Scattering Spectra of Solids*, edited by George B. Wright (Springer-Verlag, New York, 1969), p. 369.
[16]T. R. Hart, R. L. Aggarwal, and B. Lax, Phys. Rev. B 1, 638 (1970).
[17]R. A. Cowley, J. Phys. (Paris) 26, 659 (1965).
[18]P. G. Klemens, Phys. Rev. 148, 845 (1966).
[19]Melvin Lax, Phys. Rev. 138, A793 (1965).
[20]G. F. Koster, in *Solid State Physics*, edited by F. Seitz and D. Turnbull (Academic, New York, 1957), Vol. 5, p. 173.
[21]Nathan O. Folland and Franco Bassani, J. Phys. Chem. Solids 29, 281 (1968).
[22]R. J. Elliott, Phys. Rev. 96, 280 (1954).
[23]Model No. 52 Argon Ion Laser, Coherent Radiation, Palo Alto, Calif.
[24]C. E. Hathaway and Larry A. Rahn, Rev. Sci. Instr. 43, 294 (1972).
[25]Heat exchanger Model No. AC 2L 110, Air Products and Chemicals, Inc., Allentown, Pa.
[26]R. Loudon, Advan. Phys. 13, 423 (1964).
[27]D. O. Townley, Dow Corning Corp., Hemlock, Mich.
[28]J. D. Masso, Ph.D. thesis (Colorado State University, 1970) (unpublished).
[29]J. Ruvalds, Phys. Rev. B 3, 3556 (1971).
[30]J. E. Smith, Jr., M. H. Brodsky, B. L. Crowder, M. I. Nathan, and A. Pinczuk, Bull. Am. Phys. Soc. 16, 334 (1971).
[31]W. C. Dash and R. Newman, Phys. Rev. 99, 1151 (1955).
[32]G. Dolling (private communication).
[33]The various representation labels were kindly supplied by G. Dolling (private communication).
[34]L. P. Bouckaert, R. Smoluchowski, and E. Wigner, Phys. Rev. 50, 58 (1936).

PHYSICAL REVIEW B VOLUME 7, NUMBER 8 15 APRIL 1973

Phonon Tunneling Spectroscopy in *n*-Ge Schottky Barriers under Pressure*

P. Guétin† and G. Schréder‡
Laboratoires d'Electronique et de Physique Appliquée, 94-Limeil-Brévannes, France
(Received 7 September 1972)

The effect of hydrostatic pressure (up to 16.4 kbar) on the characteristics of *n*-Ge–Pb tunnel contacts has been investigated both experimentally and theoretically. The differential resistance changes only slightly because of correspondingly small changes in the main parameters. On the other hand, the magnitude of the zone-boundary-phonon structures decreases strongly as a consequence of the increase in the interband gap. An additional structure attributed to the LO(000) phonon is observed at 38.15 mV.

I. INTRODUCTION

Metal-semiconductor contacts can be successfully studied under high hydrostatic pressure, and their behavior is reasonably well accounted for in the frame of the usual tunneling model. They constitute a convenient and reliable structure which has been used in the case of *n*-GaAs[1] and *n*-GaSb.[2] In GaAs, the relatively small and smooth changes of the tunnel characteristics are due to the fact that for the range of pressure available the conduction band remains centered (Fig. 1). In GaSb, on the contrary, we have shown that the electrical characteristics exhibit huge changes due to the crossing of the Γ and *L* conduction-band extrema. For example, in the indirect-gap configuration,

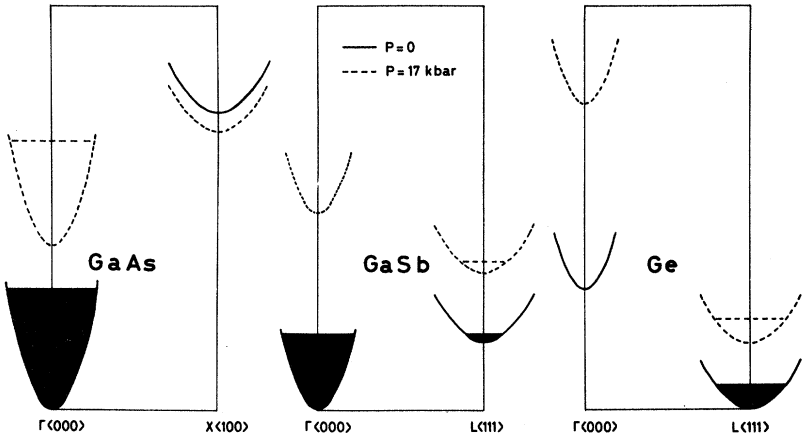

FIG. 1. Schematic drawing of the pressure-dependent positions of the *X*, Γ, and *L* conduction-band minima in Ge, GaAs, and GaSb. Fermi levels are indicated.